Much more than a toxin: hydrogen cyanide is a volatile modulator of bacterial behaviour

Abhishek Anand[1], Laurent Falquet[1,2], Eliane Abou-Mansour[1], Floriane L'Haridon[1], Christoph Keel[3] & Laure Weisskopf[1]*

[1]Department of Biology, University of Fribourg, Fribourg, Switzerland

[2]Swiss Institute of Bioinformatics, Lausanne, Switzerland

[3]Department of Fundamental Microbiology, University of Lausanne, Lausanne, Switzerland

*Correspondence:

Prof. Laure Weisskopf

Department of Biology

University of Fribourg

Chemin du musée 10

CH-1700 Fribourg

Switzerland

Tel: +41 26 300 88 11

Email: laure.weisskopf@unifr.ch

23 **Introductory paragraph**

24 **Bacteria communicate with each other and with other organisms in a chemical language**
25 **comprising both diffusible and volatile molecules, and volatiles have recently gained**
26 **increasing interest as mediators of bacterial interactions[1]. One of the first volatile**
27 **compounds discovered to play a role in biotic interactions is hydrogen cyanide (HCN)[2], a**
28 **well-known toxin, which irreversibly binds to the key respiratory enzyme cytochrome C**
29 **oxidase[3]. The main ecological function of this molecule was so far thought to lie in the**
30 **inhibition of competing microorganisms[4]. Here we show that HCN is much more than a**
31 **respiratory toxin and should be considered a major regulator of bacterial behaviour**
32 **rather than a solely defensive secondary metabolite. Cyanogenesis occurs in both**
33 **environmental and clinical *Pseudomonas* strains[5,6]. Using cyanide-deficient mutants in**
34 **two *Pseudomonas* strains, we demonstrate that HCN functions as an intracellular and**
35 **extracellular volatile signalling molecule, which leads to global transcriptome**
36 **reprogramming affecting growth, motility, and biofilm formation, as well as the**
37 **production of other secondary metabolites such as siderophores and phenazines. Our data**
38 **suggest that bacteria are using endogenous HCN not only to control their own cellular**
39 **functions, but are also able to remotely influence the behaviour of other bacteria sharing**
40 **the same environment.**

41

42

43 Cyanogenesis occurs in many different types of organisms, including bacteria, plants, animals
44 and even humans[7–9]. In bacteria, most studies have focused on *Pseudomonas* strains, which
45 form HCN by oxidative decarboxylation of glycine[4]. HCN is considered an important virulence
46 factor in both environmental (e.g. *Pseudomonas protegens* CHA0) and clinical (e.g.
47 *Pseudomonas aeruginosa* PAO1) strains[2,10]. The ecological role of HCN emission in bacterial
48 defence against competing organisms is well established and this molecule has been repeatedly
49 pinpointed as a major actor in the arsenal of root-associated *Pseudomonas* with protective
50 effects against plant diseases[11]. An earlier study using comparative genomics to identify the
51 molecular determinants of late blight control by potato-associated *Pseudomonas* highlighted
52 HCN as a likely candidate accounting for the inhibition of the devastating oomycete pathogen
53 *Phytophthora infestans*[12]. However, when we compared the anti-*Phytophthora* effects of
54 cyanogenesis-deficient mutants in two different species of *Pseudomonas* with that of their
55 respective wild types, we noticed only little to no reduction in their antagonistic potential.
56 Moreover, we observed that the mutants had gained additional antimicrobial capacities, e.g.
57 inducing higher inhibition of the pathogen's zoospore germination[13]. This prompted us to
58 quantify the mutants' secretion of siderophores, as these iron-chelators are well-known
59 mediators of antifungal activity[14]. We first grew both strains on King's B medium, which is
60 classically used to detect siderophores in pseudomonads (Figure 1a). Compared to the
61 *Escherichia coli* control, our two model strains *Pseudomonas chlororaphis* R47 and
62 *Pseudomonas putida* R32 secreted siderophores as evidenced by the halo surrounding the
63 colonies. In *P. putida* R32, the cyanide-deficient mutant appeared to produce more siderophores
64 than the wild type, while the difference was less clear for R47 in this qualitative plate assay.
65 Since we knew from these two strains' genomes that they both encoded pyoverdine production,
66 we used a fluorospectrometry-based assay[15] to quantify the production dynamics of this
67 particular siderophore as well as the growth of both wild types and mutants in liquid King's B

68 medium (Figure 1b). The production of pyoverdine was significantly higher in both the cyanide-
69 deficient mutants compared with the corresponding wild-type strains. For R47, faster growth
70 was observed for the mutant at the onset of the stationary phase, yet the strong increase in
71 pyoverdine production was in no proportion to this moderate growth advantage (Figure 1b).
72 For R32, the decreased growth of the wild type compared with the mutant was less striking and
73 only transient. This differential impact of cyanogenesis on growth in the two *Pseudomonas*
74 strains might be linked to their respective HCN production levels, which were higher (ca. 80
75 μM) for R47 than for R32 (ca. 28 μM) (Figure S1). The orange colour of R47 (Figure 1a)
76 originates from the production of phenazines, an important class of antimicrobial compounds,
77 also involved in iron acquisition, redox balance, and many other biological functions in
78 *Pseudomonas* strains[16]. We therefore also quantified the production of phenazine carboxylic
79 acid (PCA), one particular form of phenazines, in both wild-type and cyanide-deficient mutant
80 strains grown in King's B medium. We analysed this phenotype only in *P. chlororaphis* R47,
81 since phenazine biosynthetic genes are absent from the genome of *P. putida* R32. We observed
82 that similarly to pyoverdine, PCA was also produced at a higher concentration (>2.5-fold) by
83 the mutant than by the wild type (Figure 1c). Next to PCA, other phenazines were also produced
84 more abundantly in the cyanide-deficient mutant (Figure S2). Taken together, these data
85 indicate that the absence of HCN led to a significantly enhanced production of other secondary
86 metabolites that could fulfil similar ecological functions, such as the inhibition of microbial
87 competitors.
88
89 The ability to move towards a favourable environment and once there, to form a biofilm are
90 relevant features for successful colonization of both plant (e.g. root) and human (e.g. lung)
91 tissues by pseudomonads[17,18]. We therefore wondered whether motility and biofilm formation
92 would also be influenced by the loss of cyanogenesis in our two *Pseudomonas* mutants. Our

93 swimming motility assays on low agar plates revealed that both cyanide-deficient mutants were
94 significantly more motile (ca. 2-fold) than the wild types (Figure 1d). In contrast to all previous
95 phenotypes tested, where the mutants performed better than the wild types, biofilm formation
96 was significantly lower for both mutants compared to the wild types (Figure 1e). In addition to
97 confirming the expected negative relation between a motile and a sessile life style, these data
98 also provided the proof of concept that HCN also stimulated and not only inhibited
99 physiological processes in cyanogenic pseudomonads. Overall, the consistent observation in
100 two different *Pseudomonas* species that the loss of cyanogenesis led to effects as diverse as
101 enhanced siderophore production and reduced biofilm formation, confirmed our hypothesis that
102 HCN is more than a mere respiratory toxin, and likely a global regulator of bacterial physiology
103 and behaviour.
104

105 In order to test this hypothesis, we selected *P. chlororaphis* R47 because of its large genome
106 encoding many secondary metabolites[12] and compared the transcriptome of the wild type and
107 the cyanide-deficient mutant grown in liquid King's B medium at three different time points
108 (Figure 2a). We chose these time points to cover i) the early log phase, at which we did not
109 expect any change since HCN, as a secondary metabolite, was classically reported to be
110 produced at the end of the exponential growth phase[19], ii) the transition between exponential
111 and stationary growth phase, at which HCN effects were expected to start taking place, and iii)
112 the later stationary growth phase, at which we expected changes to be further amplified (Figure
113 2a). Contrary to our expectations, the transcriptomes of the wild type and the cyanide-deficient
114 mutant clustered separately already at the early log phase (Figure 2b). Looking at the expression
115 of the HCN biosynthetic operon, we observed that it was indeed expressed at the early
116 exponential phase already (Figure S3), and its absence induced the dysregulation of 32 genes
117 belonging to different COG categories at this early time point (Figure 2c and Table S1). Among

118 these, genes involved in signal transduction and lipid transport / metabolism were mainly
119 upregulated in the absence of HCN, while genes involved in transcription, amino acid and
120 carbohydrate metabolism, inorganic ion transport and secondary metabolism were mainly
121 downregulated. Genes belonging to the energy production and conversion category were also
122 dysregulated, with some being up- and others downregulated in the mutant, such as the genes
123 encoding cytochrome c oxidase orphan subunits. The early expression of alternative oxidases
124 in the wild type compared with the mutant constitutes a further proof that cyanogenesis occurs
125 earlier than classically assumed and is not solely conditioned by the lack of nutrients or of
126 oxygen occurring at the early stationary phase, where HCN production has been previously
127 reported as being maximal[4]. As expected, differences between the transcriptomes of the wild
128 type and the mutant increased over time (Figure 2b,c), with 206 genes (ca. 3.2 % of the genome)
129 dysregulated at the transition between the exponential and stationary growth phases, and 350
130 (ca. 5.5 %) at late stationary growth phase, where all COG categories were affected by the
131 presence vs. absence of HCN. These genome-wide expression changes already started at the
132 second time point (transition to stationary growth phase), where both strains still followed the
133 same growth dynamic (Figure 2a). Overall, the absence of HCN mainly led to gene
134 upregulation, as for instance the genes involved in pyoverdine and phenazine synthesis (Figure
135 2b and Table S2), which corroborated our phenotypic assays (Figure 1b). Among the few genes
136 upregulated by HCN, one was predicted to encode the helix-turn-helix-type transcriptional
137 regulator MlrA which was strongly downregulated in the cyanide-deficient mutant (Table S2).
138 In *E. coli* and *S. enterica*, MlrA was shown to activate extracellular matrix production[20]. This
139 could explain the higher biofilm forming capacity observed in the *Pseudomonas* wild types
140 compared to the cyanide-deficient mutants in the present study (Figure 1e). Higher biofilm
141 formation by wild types could also be explained by higher expression of the type VI secretion
142 system (T6SS) (Table S2). This system has been shown to be involved in biofilm formation by

143 *P. aeruginosa*[21–23]. Next to its putative role in biofilm formation, the T6SS has been involved
144 in bacterial interactions with competitors[24], similarly to HCN itself. Likewise, the operon
145 encoding the insecticidal Fit toxin[25] was also upregulated in the absence of HCN (Table S2),
146 suggesting a possible compensation of the lack of one biological weapon with the higher
147 production of others (e.g., phenazines, pyoverdine, Fit toxin and T6SS). Regarding motility,
148 transcriptomic analysis revealed upregulation of flagellar biosynthesis genes in the cyanide-
149 deficient mutant (Table S2), which could explain both the mutant's higher motility and lower
150 biofilm formation (Figure 1d,e). Altogether, the global transcriptome shifts caused by the
151 presence vs. absence of HCN corroborate the phenotypic differences observed between the wild
152 type and the cyanide-deficient mutants (Figure 1) and highlight endogenous HCN as a global
153 regulator of gene expression, compared e.g. with the global activator of secondary metabolism
154 (GacA), whose mutation led to ca 13 % of dysregulated genes in the closely related strain *P.*
155 *chlororaphis* 30-84[26]. However, the extent of the observed HCN-induced transcriptome
156 changes is in stark contrast to earlier work on *P. aeruginosa,* which reported only 16
157 dysregulated genes in an cyanide-deficient mutant[27]. This discrepancy might be due to a higher
158 resolution of RNA-Seq over microarray analysis, or to different culture conditions, with the
159 complex King's B medium in our case and glycine-enriched minimal medium in the earlier
160 study.

161 Since HCN is a gaseous molecule easily diffusing into the vicinity of cyanogenic strains, we
162 wondered whether neighbouring, non-cyanogenic cells would respond to exogenous HCN
163 supply with similar changes as those we observed between mutants and wild types. We
164 therefore carried out an experiment where the cyanide-deficient mutant of R47 was grown in
165 volatile-mediated contact with its wild type (Figure 3a, Figure S4), and compared both
166 phenotypes and transcriptomes of the wild type, the mutant and the HCN-exposed mutant.
167 Exposing the mutants of both R47 and R32 to exogenous HCN emitted by their respective wild

168 types did not impair the mutants' growth, yet it suppressed the increase in pyoverdine
169 production observed in the non-exposed mutants (Figure 3b) and restored both mutants' biofilm
170 formation and swimming motility to the wild type levels (Figure 3c,d). For the motility rescue
171 experiment, in R32 cyanide-deficient mutant, we observed swarming rather than swimming
172 motility in this split plate setup (Figure 3d). At the early exponential phase, both non-exposed
173 and exposed mutants of R47 showed similar transcriptomes (only four differentially expressed
174 genes, see Figure S5 and Table S1), suggesting that at this early time point, HCN was affecting
175 only the producing cells but was not yet diffusing into the neighbouring wells. However, at the
176 later time point corresponding to the transition between the exponential and stationary growth
177 phases, most of the gene expression changes observed in the mutant were rescued by exposure
178 to exogenous HCN (Figure 3e, Figure S5b and c). These included the changes in genes encoding
179 pyoverdine and phenazine synthesis, the insecticidal Fit toxin, as well as the MlrA activator,
180 the T6SS and the flagellar biosynthetic genes potentially involved in biofilm formation, which
181 corroborated the rescued phenotypes (Figure 3b,c,d and Table S2). The transcriptome changes
182 observed at this intermediate time point between the mutant and the exposed mutant mimicked
183 those observed between the mutant and the wild type, confirming that the exposed mutant
184 behaved largely like a wild type (Figure 3b,e). Principal component analysis showed that this
185 transcriptome similarity was further increased at the late stationary phase (time point 3),
186 although the number of dysregulated genes increased from 19 to 141, which might be due to
187 the differential growth between the wild type and the exposed mutant observed at this later time
188 point (Figure 3b, Figure S5a,b). Interestingly, the proportion of genes rescued by external
189 supply of HCN at the transition between the exponential and stationary growth phases differed
190 between the COG categories, with a lower rescue proportion in the categories involved in
191 housekeeping functions and primary metabolism (e.g., ribosome structure, replication, energy
192 production, or carbohydrate, amino acid and nucleotide metabolism) than in those potentially

193 involved in biotic interactions (e.g., defence mechanisms, inorganic ion transport and secondary
194 metabolism) (Figure S5c).

195 Altogether, our data indicate that the biological functions of HCN are much wider than
196 previously thought. Not unlike phenazines, which were also first categorized as "mere
197 secondary metabolites" and which later turned out to act as internal signalling molecules with
198 diverse and important cellular functions[28], we show here that HCN is much more than a
199 respiratory toxin, and acts as an inter- and extracellular signal on both producing and receiving
200 cells. These findings are in line with recent reports on the ability of HCN to induce broad
201 physiological effects in both plant and human cells[29,30]. Compared with phenazines, HCN is a
202 volatile molecule and as such, its zone of influence is expected to be much broader[1]. Our data
203 show that this small volatile signalling compound is able to reprogram bacterial behaviour
204 without direct contact, repressing iron uptake, swimming motility and synthesis of biological
205 weapons such as phenazines, the insecticidal Fit toxin or the type VI secretion system. These
206 functional traits are of particular interest in the competitive environments inhabited by
207 cyanogenic *Pseudomonas*, from the plant rhizosphere to the human lung, which further
208 highlights the importance of HCN not only as an intrinsic virulence factor but also, and perhaps
209 more importantly, as a volatile messenger able to manipulate the behaviour of neighbouring
210 cells to the competitive advantage of its producer.

211

212

213 **Figure legends**

214 **Figure 1 | Loss of cyanogenesis increases pyoverdine and phenazine production, induces**
215 **swimming motility and represses biofilm production.** a, Qualitative analysis of siderophore
216 production by wild-type (wt) and cyanide-deficient (Δhcn) mutant strains of both *P.*
217 *chlororaphis* R47 and *P. putida* R32 after five days of growth at room temperature on King's
218 B agar medium. Plates were visualised under UV light. b, Growth curves (optical density (OD)
219 at 600nm, lines) and pyoverdine (Pvd) detection assay (fluorescence reading at 465nm, bars) in
220 liquid King's B medium grown for 19h at 30 ˚C. Data represent the average of three independent
221 experiments with four technical replicates each. c, Phenazine quantification assay based on
222 HPLC-UV detection. R47 wt and R47 Δhcn strains were grown at 30 ˚C in liquid King's B
223 medium for 24h before sampling. Bars represent the phenazine carboxylic acid (PCA) peak
224 area normalised with growth (OD600). Data represent the average of three independent
225 experiments with three technical replicates each. d, Swimming motility assay on low agar M9
226 plates. The colony area was measured using the ImageJ software after four to five days
227 incubation at room temperature. Bars show the average of four and three independent
228 experiments for R47 and R32, respectively, with four to six technical replicates each. e, Biofilm
229 formation assay. Strains were grown statically in liquid King's B medium in 96-well plates for
230 48h at 30 ˚C. Bars correspond to biofilm index (crystal violet staining measured at 570 nm
231 divided by optical density measured at 550nm before the staining) and represent the average of
232 three independent experiments with 36 technical replicates each. For c-e, samples were
233 statistically analysed using Mann-Whitney U test (two-tailed). ***P<0.001. Error bars
234 represent standard error.

235

236 **Figure 2 | Inability to produce HCN leads to global transcriptional dysregulation.** a,
237 Representative growth curve of *P. chlororaphis* R47 wt and Δhcn strains in King's B liquid
238 medium highlighting the three time points used for transcriptome analysis. T1; early log phase,
239 T2; transition phase (exponential to stationary), T3; stationary phase. b, Principal component
240 analysis of transcriptomic data at the three time points. Strains were grown in King's B liquid
241 medium in 6-well plates at 30 ˚C with continuous shaking before each sampling. c, COG
242 category analysis of the dysregulated genes in R47 Δhcn strain compared with its wild type.
243 Bars show the percentage of dysregulated genes in each COG category. RNA-sequencing data
244 (b,c) were obtained from three independent experiments. Cut-off for significance; Log2 (fold
245 change) ≥ 1, q-value ≤ 0.05.

246

247 **Figure 3 | Exposure to exogenous HCN emitted by *P. chlororaphis* R47 wild type represses**
248 **pyoverdine production and swimming motility, but induces biofilm formation in the**
249 **cyanide-deficient mutant.** a, Scheme of the volatile-mediated exposure experiment using 6-
250 well plates used for (b). Purple color represents liquid cultures of the wild type, green color
251 liquid cultures of the cyanide-deficient mutants. The middle two wells (thicker border) were
252 collected for RNA extraction and sequencing. b, Growth (OD600) and pyoverdine (pvd)
253 measurements for *P. chlororaphis* R47 and *P. putida* R32 strains grown at 30 ˚C in liquid
254 King's B medium in 6-well plates. wt, wildtype; Δhcn, cyanide-deficient mutant; EΔhcn, Δhcn
255 strains exposed to HCN emitted by the respective wild types. Measurements were performed
256 as indicated in Figure 1. Data represent the average of three independent experiments with two

technical replicates each. T1 (early log phase), T2 (transition phase between exponential and stationary phases) and T3 (stationary phase). c, Biofilm formation assay for wild types (wt), cyanide-deficient mutants (Δhcn) and HCN-exposed mutants (EΔhcn). The assay was carried out in liquid LB as indicated in Figure 1 and Figure S6. Bars represent the average of three independent experiments with 6-20 technical replicates each. d, Swimming motility assay on split Petri dishes. The wild type and the cyanide-deficient mutant were grown on each side of the split Petri dishes (Figure S7). Plates were incubated at room temperature for two days before pictures were taken. The areas were measured as indicated in Figure 1. Bars show averages of three independent experiments with four to five technical replicates each. e, Genome-wide representation of differentially expressed genes at timepoint 2 (transition phase between exponential and stationary growth phase). The x-axis shows the gene location on the chromosome with each dot corresponding to one gene and the y-axis shows the log2 (fold change) values. (i) and (ii) log2 (fold change) values correspond to Δhcn and EΔhcn, using the wt as reference. (iii) Log2 (fold change) values correspond to the Δhcn strain using EΔhcn as reference. Red dots represent significantly differentially expressed genes while grey dots represent no significant difference as compared to the respective reference. Cut-off for significance; Log2 (fold change) ≥ 1, q-value ≤ 0.05. For b-d, samples were statistically analysed using ANOVA followed by Tukey's multiple comparison test. Error bars represent the standard error. ***$P<0.001$, **$P<0.01$, *$P<0.05$; ns, not significant. For e, dots represent average values from three independent experiments for each time point and treatment. sodA, superoxide dismutase A; hcnABC, hydrogen cyanide synthase ABC; cytochrome unit, cytochrome orphan subunit N4Q4; Pvd, pyoverdine biosynthesis genes; Phz, phenazine biosynthesis genes; glycolate, glycolate to glyoxylate oxidation; heme, heme utilisation genes; mlrA, activator of csgD (master regulator of biofilm formation) gene; Fit toxin, Fit toxin gene; GCv, glycine-cleavage system.

286 **Experimental procedures**

287 *Strains and culture media*

288 *Pseudomonas chlororaphis* (R47) and *Pseudomonas putida* (R32) and their derived Δhcn
289 mutants were grown at 30 ˚C on Lysogeny broth (LB) agar medium (20 g/L of LB mix (Lennox,
290 Fisher Bioreagents) with 15 g/L of agar (Agar-agar, Kobe I, Carl Roth))[31]. The generation of
291 Δhcn strains has been previously described[13]. King's B (KB) medium was prepared by mixing
292 20 g/L of proteose peptone #3 (Bacto™ Proteose Peptone No. 3, ThermoFisher Scientific), 1.5
293 g/L of dipotassium phosphate (Carl Roth GmbH + Co. KG), 1.5 g/L of magnesium sulfate
294 heptahydrate (Carl Roth GmbH + Co. KG) and 10ml/L of glycerol (Carl Roth GmbH + Co.
295 KG) and 15 g/L of agar (when needed).

296 *Growth curves and pyoverdine measurements*

297 Bacterial colonies (two to three single colonies) were used to inoculate LB broth and cultured
298 for 19h at 30 ˚C with shaking (180 rpm). The cells were collected by centrifugation at 5000 rpm
299 for five min and then washed twice with 0.9 % NaCl. The bacterial suspension was then
300 adjusted to OD600 = 1 (henceforth named 'OD adjusted') and 5 µl was used to inoculate 100
301 µl of KB broth in 96-well plates (Corning, NY, USA). Parafilm was used to seal the plates. A
302 Cytation5 automated plate reader (BioTek, Winooski, VT, USA) was used to incubate plates at
303 30 ˚C with continuous shaking. Reads were taken at 600 nm to generate growth curves and
304 pyoverdine measurements were done at excitation = 405 nm and emission = 460 nm[15]. For HCN
305 exposure experiments, similar readings were taken with 6-well plates (Corning, NY, USA)
306 (Figure 3a). Three ml KB broth were added to each well and 300 µl of OD adjusted bacteria
307 were added. Plates were incubated at 30 ˚C with shaking at 90 rpm and readings were taken for
308 5, 7 & 11h. All experiments were replicated three times independently in total.

309 *Phenazine measurement and identification*

310 Phenazines were quantified as previously described using a high-performance liquid
311 chromatography (HPLC) method[32]. Briefly, OD adjusted bacterial cells were inoculated in 3
312 ml King's B broth and incubated at 30 °C with shaking at 180 rpm for 24h. The culture was
313 then filtered using 0.2 µm filter (Fisher Scientific International, Inc.) and stored at -20 °C until
314 analysis. Analyses were performed by a HPLC equipped with a quaternary pump P100A,
315 coupled with a UV diode array detector ultimate 3000 (Dionex, Thermoscientific, Olten,
316 Switzerland). The samples (40 µl) were injected onto a MN Nucleosil C18 analytical column
317 (250 mm x 4 mm i.d., 100-5) (Macherey-Nagel, Duren, Germany), using a flow rate of 0.8
318 $mL.min^{-1}$ at 27 °C. The mobile phase consisted of solvent A (0.1% TFA (trifluoroacetic acid)
319 in water) and solvent B (0.1% TFA in acetonitrile); the gradient started with 5 % of solvent B
320 and reached 15 % at 2 min, 83% at 15 min, 95% at 16 min, and 100% at 45 min. Phenazines
321 were detected at 365 and 250 nm with diode array on-line detection. UV spectra were recorded
322 between 200 and 800 nm. For compound identification, samples were freeze dried, dissolved
323 in 500 µl of ethyl acetate and purified by preparative TLC on silica gel (Kieselgel 60, F_{254}, 0.25,
324 Merck, Darmstadt, Germany) using $CHCl_3$:MeOH (95:5) as the eluent. The spots were
325 visualized by exposure to UV radiation at 256 nm. Three compounds were isolated and
326 identified by HPLC and mass spectrometry as 1 or 2- hydroxyphenazine (i) (Rf 0.72; RT 14.55;
327 m/z 197.07 $[M+H]^+$), phenazine-1-carboxylic acid (PCA) (ii) (Rf 0.64; RT 1.4; m/z 225.06
328 $[M+H]^+$) and 2-hydroxyphenazine carboxylic acid (iii) (Rf 0.58; RT 21.23; m/z 241.06
329 $[M+H]^+$). ESI-MS/MS analysis in positive ionisation mode were performed on Q Exactive Plus
330 (Thermo Fisher Scientific). Mass spectra were recorded between 50 and 500 *m/z*. The peak

areas at the specific wavelength λ_{max} 250 nm were chosen for qualitative quantification. Three biologically independent replicates were collected with three technical replicates in each experiment.

Swimming motility assay

Swimming motility assays were performed as previously reported[33]. Briefly, OD adjusted inoculum was pricked into the 0.3 % M9 agar medium (For 1 litre, 10 ml of 20 % glucose (Carl Roth GmbH + Co. KG), 10 ml of 20 % casamino acids (Bacto™, Difco Laboratory), 1 ml of 1M $MgSO_4$ (Carl Roth GmbH + Co. KG), 3 g agar (Agar-agar, Kobe I, Carl Roth), 200 ml of 5X M8 solution (64 g $Na_2HPO_4.7H_2O$ (Carl Roth GmbH + Co. KG), 15 g KH_2PO_4 (Carl Roth GmbH + Co. KG), 2.5 g NaCl (Acros Organics))) in 90-mm Petri plates which were incubated in upright position for four to five days at room temperature. The experiment was replicated independently four times for R47 and three times for R32. For exposure experiments, split Petri dishes were used (Figure S7). LB agar was poured in one compartment of the dish and 0.3% M9 minimal agar medium was poured in the other compartment. Ten ml of medium was poured in each compartment of the Petri dish. The LB agar side was inoculated with three 10-µl drops of OD adjusted bacterial suspension while the M9 agar side was pricked at the centre with a pipette tip. The LB side of the plate was inoculated 6h before inoculation on the M9 agar side. Plates were parafilmed and incubated at room temperature for two days. The pictures were taken and analysed using the ImageJ software (version 1.53i)[34] to obtain the growth area in pixels square.

Biofilm formation assays

Bacterial collection and inoculation in liquid King's B medium was as described in '*Growth curves and pyoverdine measurements*'. The inoculated plates (96-well plates, Corning, NY, USA) were statically incubated at 30 ˚C for 48h and biofilm measurements were done as previously reported[35] using a Cytation5 plate reader (BioTek, Winooski, VT, USA). The experiment was replicated three times in total with 36 technical replicates each. For exposure experiments, 24-well plates (Corning, NY, USA) were used. 100 µl of OD adjusted bacterial cells were added to 1 ml of LB broth and plates were parafilmed and incubated for 48h statically at 30 ˚C. A schematic of the experimental setup is shown in Figure S6. Exposure experiments were independently reproduced three times with 6-20 technical replicates.

RNA extraction

OD adjusted bacterial cells were inoculated into 6-well plates (Corning, NY, USA) at a final OD600 of 0.1 in KB broth. The plates were then sealed with parafilm. The experimental setup is shown in Figure 3a. For all three time points, cells equivalent to OD600 = 3 were collected from the middle two wells (dark boundary in Figure 3a) by centrifugation at 5000 rpm for 5min at 4 ˚C. Samples from each treatment and time point were collected from three independent experiments. The collected cells were flash frozen using liquid nitrogen and stored at -80 ˚C until RNA extraction. RNA extraction was performed using standard phenol-chloroform extraction using the Trizol method[36]. Samples were treated with DNaseI (Sigma Aldrich) and then re-extracted using the same Trizol method as above. The RNA was quantified and analysed by the NGS facility in Bern (using both Qubit and Bioanalyser quantification). The libraries were prepared according to the TruSeq Stranded mRNA Sample Preparation Guide (Illumina). Briefly, total RNA was purified, fragmented, reverse transcribed, and amplified to generate the libraries, which were subjected to high-throughput 100bp single-end sequencing on a NovaSeq 6000 instrument (Illumina).

376 *RNA-seq data analysis*

377 Quality control of the reads was performed with FastQC v0.11.7 (fastqc:
378 https://www.bioinformatics.babraham.ac.uk/projects/fastqc/), revealing excellent quality reads
379 for all samples. The reads were cleaned using fastp v0.19.5[37] with a special focus on removing
380 polyG trails and keeping only full length reads (100bp). The reference genome for
381 *Pseudomonas chlororaphis* R47 (CP019399) was downloaded from the NCBI data analysis and
382 indexed for STAR v2.5.0b[38]. Then the reads of each sample from step 1 were remapped to
383 genes with STAR using the annotation information (gtf file). The final table of counts was
384 obtained by merging the individual tables with unix commands. The read counts were then
385 analysed using the R library DESeq2, version 1.30.1[39]. The Log2 (fold change) cut-off was set
386 to greater than or equal to 1 and the adjusted p-value threshold was set to less or equal to 0.05.

387 *qPCR analysis*

388 Three biologically independent samples collected for RNA-seq were analysed for the
389 expression of the *hcnA* gene. Primers used are described in Table S3. RNA samples were
390 reverse transcribed using the SensiFAST cDNA synthesis kit (Bioline). Quantitative PCR was
391 performed according to the manufacturer's instructions (Bioline). Briefly, 25 ng of cDNA was
392 mixed with 0.5 µl of forward and reverse primers (10 µM), 1.5 µl of sterile water and 7.5 µl
393 SYBR Hi-ROX mix (Bioline). Reaction conditions were as follows; 95 ˚C for 15min (initial
394 denaturation), 45 cycles of 95 ˚C for 15s, 60 ˚C for 15s, 72 ˚C for 30s. Data were analysed using
395 the delta Cq method.

396 *Hydrogen cyanide quantification*

397 R47 and R32 wild-type strains were inoculated and grown in 6-well plates as described in the
398 *RNA extraction* section except that the middle two wells were inoculated with 1 ml 0.38 M
399 NaOH (Merck, Germany) to capture HCN in the surrounding. At the transition phase between
400 exponential and stationary growth, the experiment was stopped, the OD600 was measured using
401 Cytation5 automated plate reader and NaOH was collected. In a 96-well plate aliquots of 100
402 µl of collected NaOH sample were mixed with 100 µl of 1 M HCl (Fisher Scientific U.K. Ltd)
403 and immediately covered with HCN detection filter paper[13]. After 30 min incubation at room
404 temperature, the filter paper was scanned using Epson Perfection V370 Photo scanner and
405 analysed using ImageJ image analysis software. A standard curve was made with KCN (Merck,
406 Germany) solution of 31, 62 and 125 µM in 0.38 M NaOH. The experiment was replicated
407 three times independently.

408 *Statistical analysis*

409 All statistical analyses for phenotypic assays were performed using Graphpad Prism 8.0.1
410 (https://www.graphpad.com/). For pair-wise comparisons, the Mann-Whitney test was done
411 (Figure 1c-e). For multiple comparisons, the linear model assumptions were checked and
412 ANOVA followed by Tukey's test was used for analysis (data was log transformed for Figure
413 3d).

References

1. Weisskopf, L., Schulz, S. & Garbeva, P. Microbial volatile organic compounds in intra-kingdom and inter-kingdom interactions. *Nature Reviews Microbiology* **19** 391–404 (2021).
2. Voisard, C., Keel, C., Haas, D. & Dèfago, G. Cyanide production by *Pseudomonas fluorescens* helps suppress black root rot of tobacco under gnotobiotic conditions . *EMBO J.* **8**, 351–358 (1989).
3. Wilson, M. T., Antonini, G., Malatesta, F., Sarti, P. & Brunori, M. Probing the oxygen binding site of cytochrome c oxidase by cyanide. *J. Biol. Chem.* **269**, 24114–24119 (1994).
4. Blumer, C. & Haas, D. Mechanism, regulation, and ecological role of bacterial cyanide biosynthesis. *Arch. Microbiol.* **173**, 170–177 (2000).
5. Ryall, B., Davies, J. C., Wilson, R., Shoemark, A. & Williams, H. D. *Pseudomonas aeruginosa*, cyanide accumulation and lung function in CF and non-CF bronchiectasis patients. *Eur. Respir. J.* **32**, 740–747 (2008).
6. Haas, D. & Défago, G. Biological control of soil-borne pathogens by fluorescent pseudomonads. *Nature Reviews Microbiology* **3** 307–319 (2005).
7. Gunasekar, P. G., Borowitz, J. L., Turek, J. J., Van Horn, D. A. & Isom, G. E. Endogenous generation of cyanide in neuronal tissue: Involvement of a peroxidase system. *J. Neurosci. Res.* **61**, 570–575 (2000).
8. Bröckner, A. *et al.* Storage and release of hydrogen cyanide in a chelicerate (*Oribatula tibialis*). *Proc. Natl. Acad. Sci. U. S. A.* **114**, 3469–3472 (2017).
9. Peiser, G. D. *et al.* Formation of cyanide from carbon 1 of 1-aminocyclopropane-1-carboxylic acid during its conversion to ethylene. *Proc. Natl. Acad. Sci.* **81**, 3059–3063 (1984).
10. Williams, H. D., Zlosnik, J. E. A. & Ryall, B. Oxygen, cyanide and energy generation in the cystic fibrosis pathogen *Pseudomonas aeruginosa*. *Advances in Microbial Physiology* **52** (2006).
11. Zdor, R. E. Bacterial cyanogenesis: Impact on biotic interactions. *J. Appl. Microbiol.* **118**, 267–274 (2015).
12. De Vrieze, M. *et al.* Linking comparative genomics of nine potato-associated *Pseudomonas* isolates with their differing biocontrol potential against late blight. *Front. Microbiol.* **11**, 857 (2020).
13. Anand, A. *et al.* Contribution of hydrogen cyanide to the antagonistic activity of *pseudomonas* strains against *phytophthora infestans*. *Microorganisms* **8**, 1–10 (2020).
14. Kloepper, J. W., Leong, J., Teintze, M. & Schroth, M. N. Enhanced plant growth by siderophores produced by plant growth-promoting rhizobacteria. *Nature* **286**, 885–886 (1980).

15. Kang, D. & Kirienko, N. V. High-throughput genetic screen reveals that early attachment and biofilm formation are necessary for full pyoverdine production by *Pseudomonas aeruginosa*. *Front. Microbiol.* **8**, 1–15 (2017).

16. Mavrodi, D. V., Blankenfeldt, W. & Thomashow, L. S. Phenazine compounds in fluorescent *Pseudomonas spp*. biosynthesis and regulation. *Annu. Rev. Phytopathol.* **44**, 417–445 (2006).

17. O'Toole, G., Kaplan, H. B. & Kolter, R. Biofilm formation as microbial development. *Annual Review of Microbiology* **54** 49–79 (2000).

18. Morris, C. E. & Monier, J. M. The ecological significance of biofilm formation by plant-associated bacteria. *Annual Review of Phytopathology* **41** 429–453 (2003).

19. Castric, P. A. Hydrogen cyanide, a secondary metabolite of *Pseudomonas aeruginosa*. *Can. J. Microbiol.* **21**, 613–618 (1975).

20. Brown, P. K. *et al.* MIrA, a novel regulator of curli (AgF) and extracellular matrix synthesis by *Escherichia coli* and Salmonella enterica *serovar typhimurium*. *Mol. Microbiol.* **41**, 349–363 (2001).

21. Southey-Pillig, C. J., Davies, D. G. & Sauer, K. Characterization of temporal protein production in *Pseudomonas aeruginosa* biofilms. *J. Bacteriol.* **187**, 8114–8126 (2005).

22. Cascales, E. The type VI secretion toolkit. *EMBO Rep.* **9**, 735–41 (2008).

23. Gallique, M., Bouteiller, M. & Merieau, A. The type VI secretion system: A dynamic system for bacterial communication? *Front. Microbiol.* **8**, 1–10 (2017).

24. Coulthurst, S. The Type VI secretion system: A versatile bacterial weapon. *Microbiol. (United Kingdom)* **165**, 503–515 (2019).

25. Flury, P. *et al.* Insect pathogenicity in plant-beneficial pseudomonads: Phylogenetic distribution and comparative genomics. *ISME J.* **10**, 2527–2542 (2016).

26. Wang, D. *et al.* Roles of the Gac-Rsm pathway in the regulation of phenazine biosynthesis in *Pseudomonas chlororaphis* 30-84. *Microbiologyopen* **2**, 505–524 (2013).

27. Frangipani, E., Pérez-Martínez, I., Williams, H. D., Cherbuin, G. & Haas, D. A novel cyanide-inducible gene cluster helps protect *Pseudomonas aeruginosa* from cyanide. *Environ. Microbiol. Rep.* **6**, 28–34 (2014).

28. Price-Whelan, A., Dietrich, L. E. P. & Newman, D. K. Rethinking 'secondary' metabolism: Physiological roles for phenazine antibiotics. *Nat. Chem. Biol.* **2**, 71–78 (2006).

29. Randi, E. B., Zuhra, K., Pecze, L., Panagaki, T. & Szabo, C. Physiological concentrations of cyanide

474 stimulate mitochondrial Complex IV and enhance cellular bioenergetics. *Proc. Natl. Acad. Sci. U. S. A.*
475 **118**, (2021).
476 30. García, I., Arenas-Alfonseca, L., Moreno, I., Gotor, C. & Romero, L. C. HCN regulates cellular
477 processes through posttranslational modification of proteins by s-cyanylation. *Plant Physiol.* **179**, 107–
478 123 (2019).
479 31. Hunziker, L. *et al. Pseudomonas* strains naturally associated with potato plants produce volatiles with
480 high potential for inhibition of *Phytophthora infestans*. *Appl. Environ. Microbiol.* **81**, 821–830 (2015).
481 32. Kern, S. E. & Newman, D. K. Measurement of phenazines in bacterial cultures. *Methods Mol. Biol.*
482 **1149**, 303–310 (2014).
483 33. Ha, D. G., Kuchma, S. L. & O'Toole, G. A. Plate-based assay for swimming motility in *pseudomonas*
484 *aeruginosa*. *Methods Mol. Biol.* **1149**, 59–65 (2014).
485 34. Schneider, C. A., Rasband, W. S. & Eliceiri, K. W. NIH Image to ImageJ: 25 years of image analysis.
486 *Nature Methods* vol. 9 671–675 (2012).
487 35. Coffey, B. M. & Anderson, G. G. Biofilm formation in the 96-well microtiter plate. *Methods Mol. Biol.*
488 **1149**, 631–641 (2014).
489 36. Chomczynski, P. & Sacchi, N. Single-step method of RNA isolation by acid guanidinium thiocyanate-
490 phenol-chloroform extraction. *Anal. Biochem.* **162**, 156–159 (1987).
491 37. Chen, S., Zhou, Y., Chen, Y. & Gu, J. Fastp: An ultra-fast all-in-one FASTQ preprocessor. in
492 *Bioinformatics* vol. 34 i884–i890 (2018).
493 38. Dobin, A. *et al.* STAR: Ultrafast universal RNA-seq aligner. *Bioinformatics* **29**, 15–21 (2013).
494 39. Love, M. I., Huber, W. & Anders, S. Moderated estimation of fold change and dispersion for RNA-seq
495 data with DESeq2. *Genome Biol.* **15**, (2014).
496
497

Acknowledgements

Financial support from the Swiss National Science Foundation (grant 179310 to LW) is gratefully acknowledged. We also thank Mout de Vrieze for her help with statistical analyses.

Author Contributions

LW and AA conceived the project and wrote the manuscript, with help from CK. AA performed all experiments, with help from FLH. LF performed transcriptomics analysis, EAM performed HPLC analysis. All authors commented on the manuscript.

Competing Interests statement

The authors declare no competing interests.

Figure 1

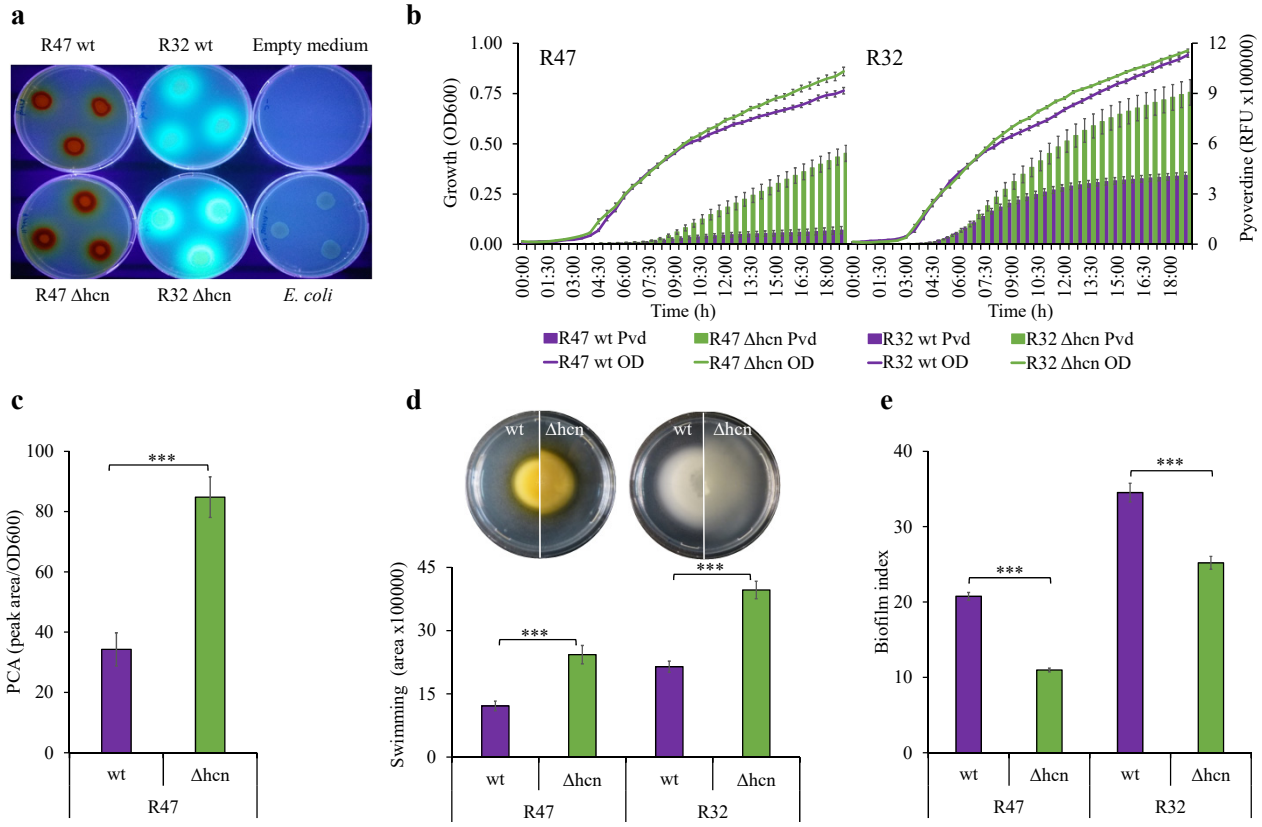
a
R47 wt
R32 wt
Empty medium
R47 Δhcn
R32 Δhcn
E. coli
b
R47
R32
Growth (OD600)
Pyoverdine (RFU x100000)
Time (h)
R47 wt Pvd
R47 Δhcn Pvd
R32 wt Pvd
R32 Δhcn Pvd
R47 wt OD
R47 Δhcn OD
R32 wt OD
R32 Δhcn OD
c
PCA (peak area/OD600)
***
wt
Δhcn
R47
d
wt
Δhcn
Swimming (area x100000)
***
R47
R32
e
Biofilm index
***
R47
R32

Figure 2

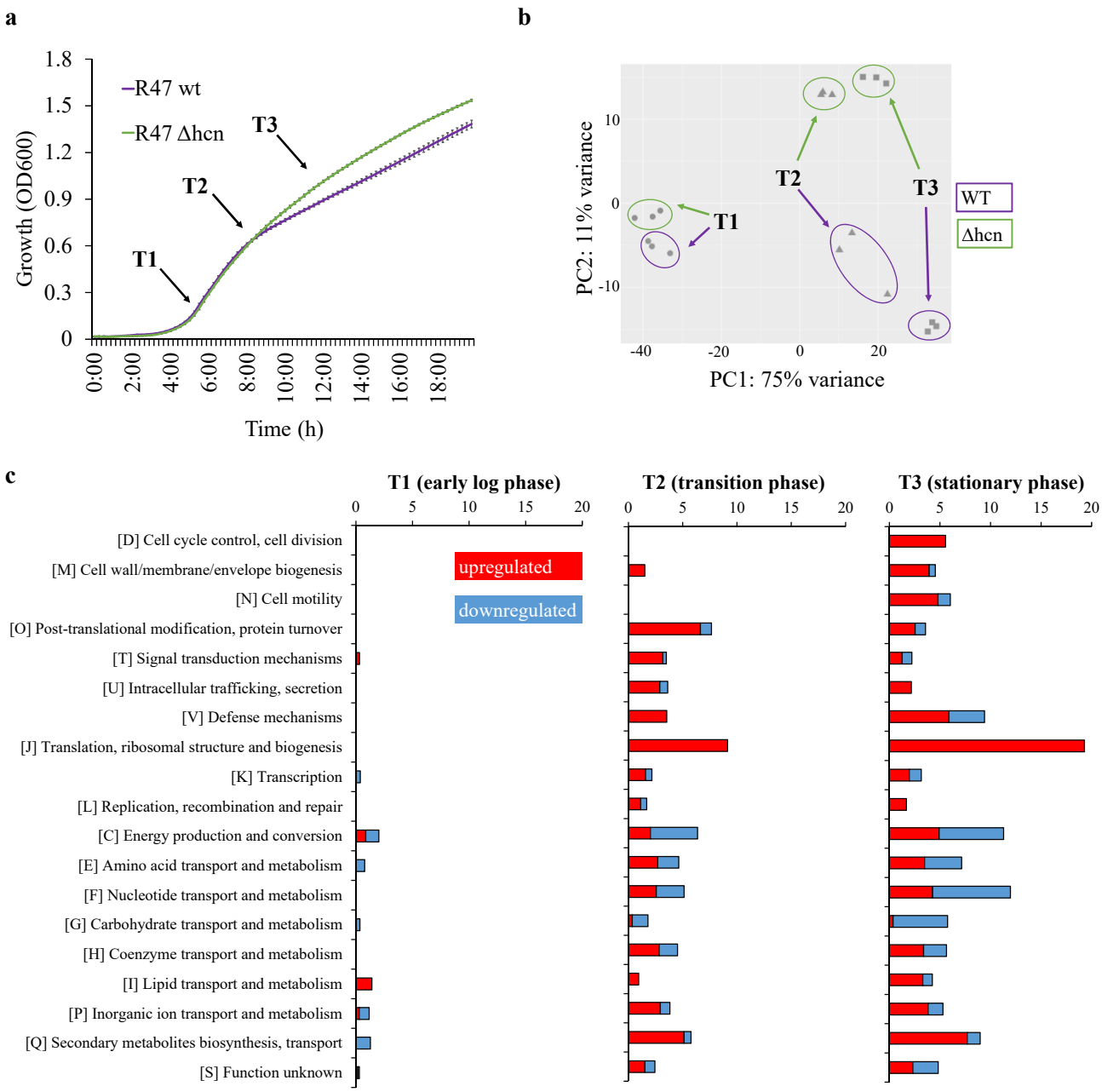
a
Growth (OD600)
Time (h)
R47 wt
R47 Δhcn
T1
T2
T3
b
PC2: 11% variance
PC1: 75% variance
T1
T2
T3
WT
Δhcn
c
T1 (early log phase)
T2 (transition phase)
T3 (stationary phase)
upregulated
downregulated
[D] Cell cycle control, cell division
[M] Cell wall/membrane/envelope biogenesis
[N] Cell motility
[O] Post-translational modification, protein turnover
[T] Signal transduction mechanisms
[U] Intracellular trafficking, secretion
[V] Defense mechanisms
[J] Translation, ribosomal structure and biogenesis
[K] Transcription
[L] Replication, recombination and repair
[C] Energy production and conversion
[E] Amino acid transport and metabolism
[F] Nucleotide transport and metabolism
[G] Carbohydrate transport and metabolism
[H] Coenzyme transport and metabolism
[I] Lipid transport and metabolism
[P] Inorganic ion transport and metabolism
[Q] Secondary metabolites biosynthesis, transport
[S] Function unknown

Figure 3

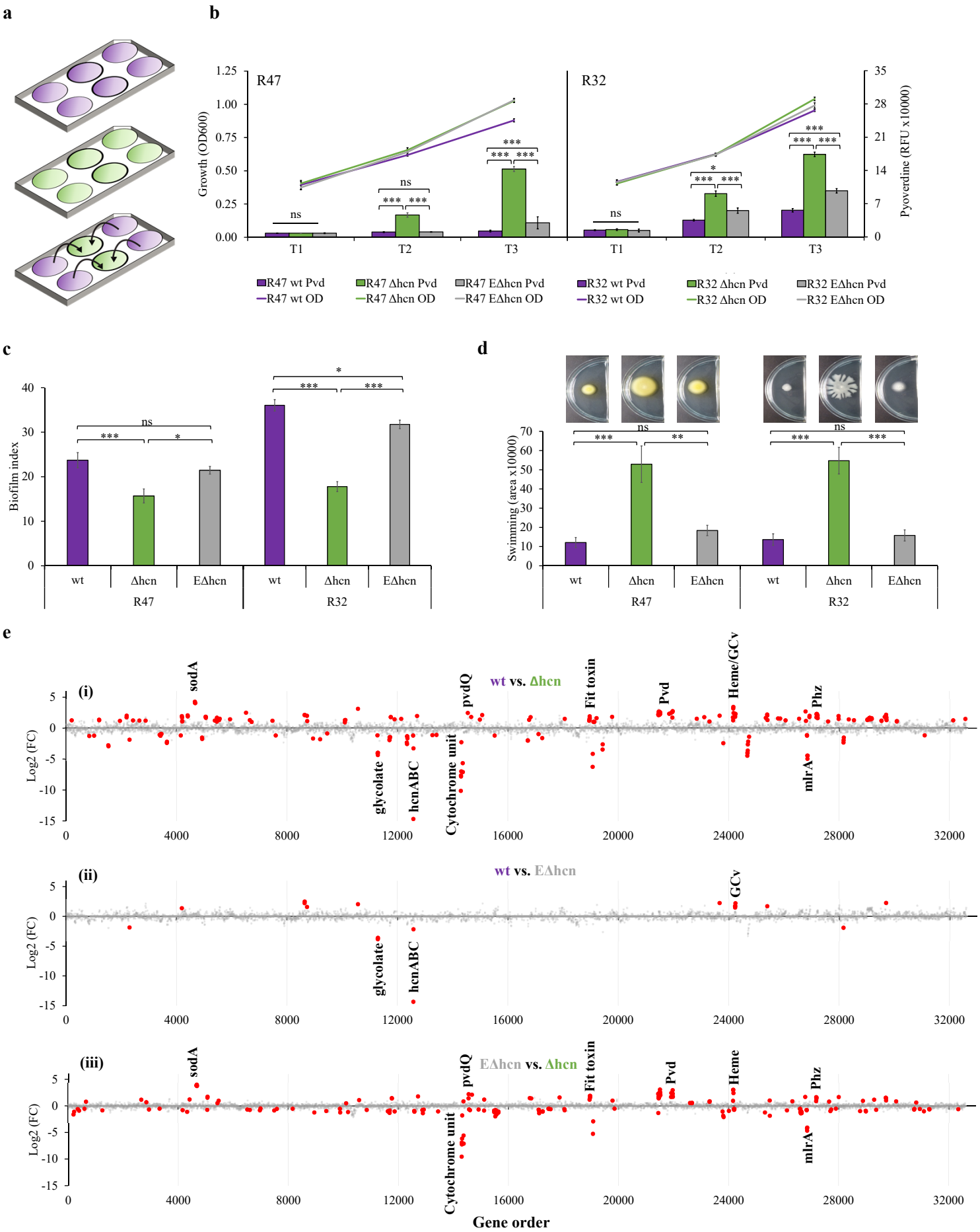
a
b
R47
R32
Growth (OD600)
Pyoverdine (RFU x10000)
T1
T2
T3
ns
***
*
R47 wt Pvd
R47 Δhcn Pvd
R47 EΔhcn Pvd
R47 wt OD
R47 Δhcn OD
R47 EΔhcn OD
R32 wt Pvd
R32 Δhcn Pvd
R32 EΔhcn Pvd
R32 wt OD
R32 Δhcn OD
R32 EΔhcn OD
c
Biofilm index
wt
Δhcn
EΔhcn
R47
R32
d
Swimming (area x10000)
e
(i)
wt vs. Δhcn
sodA
glycolate
hcnABC
Cytochrome unit
pvdQ
Fit toxin
Pvd
Heme/GCv
mlrA
Phz
Log2 (FC)
(ii)
wt vs. EΔhcn
GCv
(iii)
EΔhcn vs. Δhcn
Heme
Gene order